Capacitance Reduction of the Hybrid Modular Multilevel Converter by Decreasing Average Capacitor Voltage in Variable-Speed Drives

Shaoze Zhou, *Student Member, IEEE*, Binbin Li, *Member, IEEE*, Mingxu Guan, Xinyi Zhang, Zigao Xu, *Student Member, IEEE*, and Dianguo Xu, *Fellow, IEEE*

***Abstract*—Modular multilevel converters (MMCs) represent an emerging topology in medium-voltage (MV) and high-voltage applications. But for MV variable-speed motor drives, the MMC faces the challenge of large capacitor voltage ripple at low speeds. Delightfully, a hybrid MMC (HMMC) has proved to be potential in MV motor drives, since this topology has a lower capacitor voltage ripple and does not introduce any common voltage to the motor. This paper proposed a method to decrease the average capacitor voltage of the HMMC, which can effectively drive the motor at very low speeds without significantly increasing the submodule (SM) capacitance. Moreover, the selection of average capacitor voltage and the dimension of the SM capacitance are presented. Simulation and experimental results verify the effectiveness of the proposed method.**

***Index Terms*—Average capacitor voltage, capacitance reduction, hybrid topology, modular multilevel converter (MMC), variable-speed drives.**

I. Introduction

MODULAR multilevel converters (MMCs) have recently drawn increasing attention in medium-voltage (MV) variable-speed motor drives [1]–[6]. The main problem of the MMC in this application is the submodule (SM) capacitor voltage ripple, which is in proportion with the output current and inversely proportional to the output frequency. Hence, at low motor speed with high-torque requirements, the capacitor voltage ripple will be unacceptably large and the required capacitance increases. Antonopoulos *et al.* [7] proposed reducing the average capacitor voltage to tolerate a larger capacitor voltage

Manuscript received March 26, 2018; accepted April 29, 2018. Date of publication May 6, 2018; date of current version December 7, 2018. This work was supported in part by the National Natural Science Foundation of China under Grant 51477034 and Grant 51720105008, in part by the Power Electronics Science and Education Development Program of Delta Group, and in part by the Young Elite Scientists Sponsorship Program by China Association for Science and Technology. Recommended for publication by Associate Editor A. Mertens. *(Corresponding author: Binbin Li.)*

S. Zhou, B. Li, M. Guan, Z. Xu, and D. Xu are with the School of Electrical Engineering and Automation, Harbin Institute of Technology, Harbin 150001, China (e-mail:

voltage ripple and does not inject harmful common-mode voltage nor circulating current. However, the capacitor voltage ripple of the HMMC at very low speed is still higher (at least twice of that at rated speed), which also calls for a larger capacitance. To solve this problem, an operation of decreasing the average capacitor voltage is proposed in this paper, which can tolerate large capacitor voltage ripple even at very low speed. The contribution of this paper is truly realizing the MMC variable-speed motor drive without significantly increasing the SM capacitance. Compared with existing literatures, the proposed method can achieve a significant reduction of the capacitance and is very valuable for engineering. Correspondingly, determination of the average capacitor voltage is presented, while dimension of the capacitance by including the average capacitor voltage as a factor is also proposed.

The remainder of this paper consists of the following. In Section II, the mathematical expression of the HMMC capacitor voltage ripple is derived. Section III proposes the average capacitor voltage decrease operation, including the optimal selection of this average capacitor voltage and dimension of the SM capacitance. Then, simulation and experimental results are given in Section IV, which demonstrate validity of the proposed method. Finally, Section V concludes this paper.

II. Analysis of the HMMC Capacitor Voltage Ripple

A. Basics of the HMMC Topology

Circuit configuration of the HMMC is shown in Fig. 1(a). A series switch (S_s) is inserted between the MMC and the dc voltage source. This switch is used to disconnect the MMC with the dc source at regular intervals, and the dc current ($i_{\rm dc}$) is controlled as a square waveform. Due to the controllability of $i_{\rm dc}$, the series switch can be soft switched and thyristors can be used [22].

Considering one of the phases, the output ac voltage and current are assumed to be sinusoidal

$$u_o = U_{\rm OM}\cos(\omega t) = \frac{1}{2}mU_{\rm dc}\cos(\omega t) \tag{1}$$

$$i_o = I_{\rm OM}\cos(\omega t - \varphi) \tag{2}$$

where m is the modulation index, $U_{\rm dc}$ is the dc source voltage, $U_{\rm OM}$ and $I_{\rm OM}$ are the amplitudes of the output voltage and current, respectively, ω is the output angular frequency, and φ is the phase lag angle. When a constant-load-torque motor is connected, $I_{\rm OM}$ is constant.

As in motor drive applications, a constant m/ω ratio (i.e., volt/hertz ratio) is approximately ensured, which gives

$$m = \frac{m_{\rm rated}}{\omega_{\rm rated}}\omega \tag{3}$$

where $m_{\rm rated}$ and $\omega_{\rm rated}$ are modulation index and output angle frequency at rated motor speed, respectively. Due to the impact of capacitor voltage ripples in the MMC, $m_{\rm rated}$ is around 0.8–1. In practical motor drive applications, m/ω ratio is not always ensured at a low frequency. The converter sometimes needs to output an extra voltage to compensate for the voltage drop across the motor stator. In this case, we can use

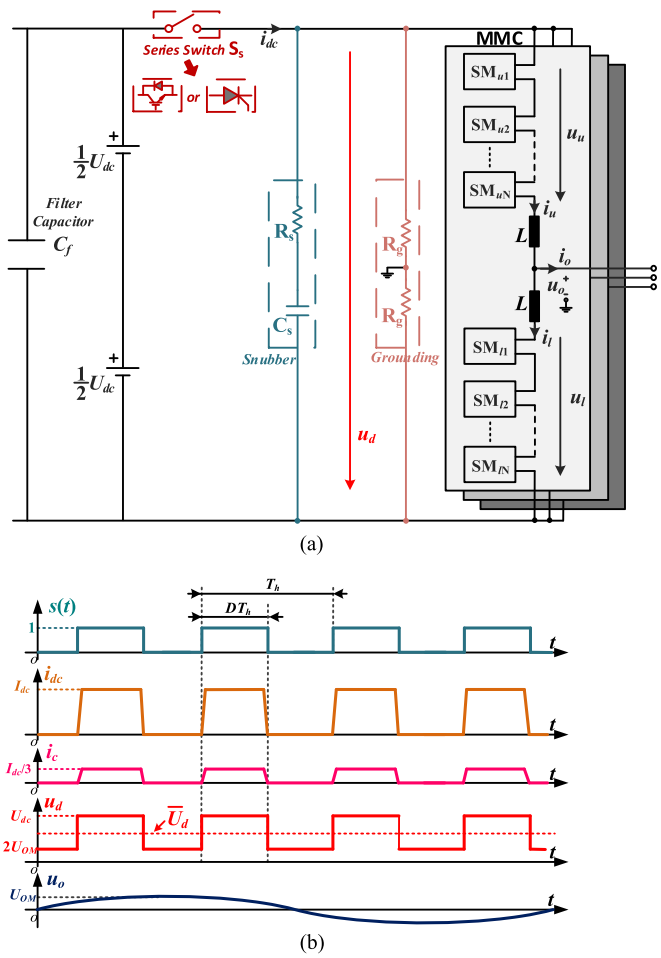

Fig. 1. (a) Circuit configuration of the HMMC. (b) Sketch map of the operation waveforms of the HMMC.

"$m = K(\omega - \omega_{\rm rated}) + m_{\rm rated}$" to replace (3), where slope K reflects the extent of compensation voltage. Here, (3) is selected to simplify the analysis in this paper.

As shown in Fig. 1(b), for the series switch S_s switching at frequency of f_h ($f_h = 1/T_h$) with duty cycle D, the switching function can be expressed as follows:

$$s(t) = \begin{cases} 0, & 0 \le t < (1-D)T_h \\ 1, & (1-D)T_h \le t < T_h. \end{cases} \tag{4}$$

The dc current of the HMMC can be expressed as $i_{\rm dc} = I_{\rm dc}s(t)$ with

$$I_{\rm dc} = \frac{3}{4}m_{\rm rated}I_{\rm OM}\cos\varphi. \tag{5}$$

When the motor speed varies, balance of the active power between dc and ac terminals is achieved by adjusting the duty cycle D: $U_{\rm dc}I_{\rm dc}D = 1.5U_{\rm OM}I_{\rm OM}\cos\varphi$. Hence, for constant-torque drives with constant $I_{\rm OM}$, D can be derived as follows:

$$D = \frac{\omega}{\omega_{\rm rated}}. \tag{6}$$

The characteristic of the HMMC is that when the series switch S_s is turned OFF, the dc voltage component of the HMMC u_d is

reduced to $2U_{\rm OM}$, as shown in Fig. 1(b), which gives

$$u_d = s(t)U_{\rm dc} + [1 - s(t)]\,2U_{\rm OM}. \tag{7}$$

Then, the arm voltages and currents of the HMMC can be expressed as follows:

$$\begin{cases} u_u = \frac{1}{2}u_d - u_o = \frac{1}{2}U_{\rm dc} \\ \qquad \left\{ s(t) + [1 - s(t)]\,\frac{m_{\rm rated}}{\omega_{\rm rated}}\omega - \frac{m_{\rm rated}}{\omega_{\rm rated}}\omega\cos(\omega t) \right\} \\ u_l = \frac{1}{2}u_d + u_o = \frac{1}{2}U_{\rm dc} \\ \qquad \left\{ s(t) + [1 - s(t)]\,\frac{m_{\rm rated}}{\omega_{\rm rated}}\omega + \frac{m_{\rm rated}}{\omega_{\rm rated}}\omega\cos(\omega t) \right\} \end{cases} \tag{8}$$

$$\begin{cases} i_u = \frac{1}{3}i_{\rm dc} + \frac{1}{2}i_o = \frac{1}{4}m_{\rm rated}I_{\rm OM}s(t)\cos\varphi \\ \qquad + \frac{1}{2}I_{\rm OM}\cos(\omega t - \varphi) \\ i_l = \frac{1}{3}i_{\rm dc} - \frac{1}{2}i_o = \frac{1}{4}m_{\rm rated}I_{\rm OM}s(t)\cos\varphi \\ \qquad - \frac{1}{2}I_{\rm OM}\cos(\omega t - \varphi). \end{cases} \tag{9}$$

The ratings of the HMMC are briefly discussed here. The current stress of S_s is the amplitude of dc current (which is always $I_{\rm dc}$), as shown in (5). The voltage of S_s is the difference between dc source and dc voltage seen by the MMC circuit, which is, according to (7), $U_{\rm dc}- 2U_{\rm OM}$. Since $U_{\rm OM}$ would be very small during low motor speeds, the voltage rating of S_s needs to be designed as $U_{\rm dc}$. With respect to the insulated gate bipolar transistor (IGBT) requirements in the SMs, according to (9), the arm current stress can remain the rated value $(1/2I_{\rm OM} + 1/3I_{\rm dc})$ within the whole speed range. Hence, the SM IGBTs do not need to be oversized compared with the existing circulating current injection methods.

B. Capacitor Voltage Ripple Analysis

In the HMMC, the average SM capacitor voltage U_C is normally kept balanced at the rated value $U_{C(\rm rated)}$ ($U_{C(\rm rated)} = U_{\rm dc}/N$). The insertion indexes of the upper and lower arms are

$$\begin{cases} n_u = \dfrac{u_u}{NU_{C(\rm rated)}} \\ \quad = \dfrac{1}{2}s(t) + \dfrac{1}{2}[1 - s(t)]\,\dfrac{m_{\rm rated}}{\omega_{\rm rated}}\omega - \dfrac{1}{2}\dfrac{m_{\rm rated}}{\omega_{\rm rated}}\omega\cos(\omega t) \\ n_l = \dfrac{u_l}{NU_{C(\rm rated)}} \\ \quad = \dfrac{1}{2}s(t) + \dfrac{1}{2}[1 - s(t)]\,\dfrac{m_{\rm rated}}{\omega_{\rm rated}}\omega + \dfrac{1}{2}\dfrac{m_{\rm rated}}{\omega_{\rm rated}}\omega\cos(\omega t). \end{cases} \tag{10}$$

Then, the current flowing through the capacitor of each SM can be obtained by

$$\begin{cases} i_{Cu} = n_u i_u \\ i_{Cl} = n_l i_l. \end{cases} \tag{11}$$

Substituting (9) and (10) into (11) yields

$$\begin{cases} i_{Cu} = \frac{I_{\rm OM}}{4} \\ \times \begin{Bmatrix} \cos(\omega t - \varphi)s(t) + \frac{m_{\rm rated}}{\omega_{\rm rated}}\omega\cos(\omega t - \varphi)[1 - s(t)] \\ -\frac{m_{\rm rated}^2\cos\varphi}{2\omega_{\rm rated}}\omega\cos(\omega t)s(t) - \frac{m_{\rm rated}}{2\omega_{\rm rated}}\omega\cos(2\omega t - \varphi) \\ -\frac{m_{\rm rated}\cos\varphi}{2\omega_{\rm rated}}\omega + \frac{m_{\rm rated}\cos\varphi}{2}s(t) \end{Bmatrix} \\ i_{Cl} = \frac{I_{\rm OM}}{4} \\ \times \begin{Bmatrix} -\cos(\omega t - \varphi)s(t) - \frac{m_{\rm rated}}{\omega_{\rm rated}}\omega\cos(\omega t - \varphi)[1 - s(t)] \\ +\frac{m_{\rm rated}^2\cos\varphi}{2\omega_{\rm rated}}\omega\cos(\omega t)s(t) - \frac{m_{\rm rated}}{2\omega_{\rm rated}}\omega\cos(2\omega t - \varphi) \\ -\frac{m_{\rm rated}\cos\varphi}{2\omega_{\rm rated}}\omega + \frac{m_{\rm rated}\cos\varphi}{2}s(t) \end{Bmatrix} \end{cases}. \tag{12}$$

Since f_h is generally ten times higher than the output frequency f ($f = \omega/(2\pi)$). In steady state, it is reasonable to approximate $s(t)$ by its average value D. Substituting D by (6), (12) becomes

$$\begin{cases} i_{Cu} \approx \frac{I_{\rm OM}}{4\omega_{\rm rated}} \\ \times \begin{Bmatrix} -\frac{m_{\rm rated}}{2}\omega\cos(2\omega t - \varphi) - \frac{m_{\rm rated}^2\cos\varphi}{2\omega_{\rm rated}}\omega^2\cos(\omega t) \\ +\omega\left(1 + m_{\rm rated}\frac{\omega_{\rm rated} - \omega}{\omega_{\rm rated}}\right)\cos(\omega t - \varphi) \end{Bmatrix} \\ i_{Cl} \approx \frac{I_{\rm OM}}{4\omega_{\rm rated}} \\ \times \begin{Bmatrix} -\frac{m_{\rm rated}}{2}\omega\cos(2\omega t - \varphi) + \frac{m_{\rm rated}^2\cos\varphi}{2\omega_{\rm rated}}\omega^2\cos(\omega t) \\ -\omega\left(1 + m_{\rm rated}\frac{\omega_{\rm rated} - \omega}{\omega_{\rm rated}}\right)\cos(\omega t - \varphi) \end{Bmatrix} \end{cases}. \tag{13}$$

Then, capacitor voltage ripples of each SM can be obtained by integrating (13)

$$\begin{cases} \Delta u_{Cu} = \frac{1}{C}\int i_{Cu}dt \\ = \frac{I_{\rm OM}}{4\omega_{\rm rated}C}\begin{Bmatrix} -\frac{m_{\rm rated}}{4}\sin(2\omega t - \varphi) - \frac{m_{\rm rated}^2\cos\varphi}{2\omega_{\rm rated}}\omega\sin(\omega t) \\ +\left(1 + m_{\rm rated}\frac{\omega_{\rm rated} - \omega}{\omega_{\rm rated}}\right)\sin(\omega t - \varphi) \end{Bmatrix} \\ \Delta u_{Cl} = \frac{1}{C}\int i_{Cl}dt \\ = \frac{I_{\rm OM}}{4\omega_{\rm rated}C}\begin{Bmatrix} -\frac{m_{\rm rated}}{4}\sin(2\omega t - \varphi) + \frac{m_{\rm rated}^2\cos\varphi}{2\omega_{\rm rated}}\omega\sin(\omega t) \\ -\left(1 + m_{\rm rated}\frac{\omega_{\rm rated} - \omega}{\omega_{\rm rated}}\right)\sin(\omega t - \varphi) \end{Bmatrix} \end{cases} \tag{14}$$

where the voltage ripple contains fundamental and second-order components. With respect to the second-harmonic component, its amplitude is U_{C2} $(= I_{\rm OM}m_{\rm rated}/(16\omega_{\rm rated}C))$. Fig. 2 compares U_{C2} with the fundamental component U_{C1} [the expression of U_{C1} will be shown in (16)] in full frequency range. (The parameters are the same as the simulation in Section IV, as shown in Table I.) It can be seen that U_{C2} is invariant with frequency and is about 10%–20% of U_{C1}. Hence, by introducing some margin voltage when designing the SM capacitance, U_{C2} can be neglected for simplicity.

Thus, the fundamental component dominates; then, Δu_{Cu} and Δu_{Cl} can be simplified as follows:

$$\begin{cases} \Delta u_{Cu} \approx U_{C1}\sin(\omega t + \theta) \\ \Delta u_{Cl} \approx -U_{C1}\sin(\omega t + \theta) \end{cases} \tag{15}$$

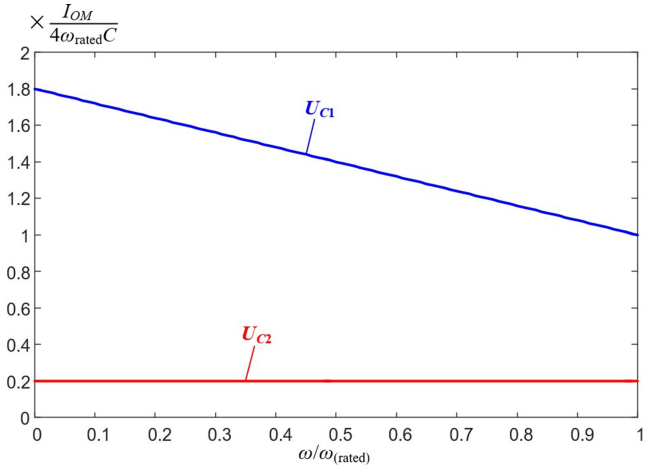

Fig. 2. Comparison between U_{C1} and U_{C2} in full frequency ranges.

TABLE I
SIMULATION PARAMETERS

HMMC parameters	
Number of SMs per arm	N=10
DC-source voltage	U_{dc}=8000V
Rated SM average capacitor voltage	$U_{C(\text{rated})}$=800V
SM capacitor peak voltage limit	U_{limit}=840V
Margin voltage	ΔU=880V
SM capacitance	C=4mF
Arm inductance	L=1mH
Rated output frequency	f_{rated}=50Hz
Rated modulation index	m_{rated}=0.8
Rated phase current magnitude	I_{OM}=250A
Rated dc current	I_{dc}=150A
Switching frequency of each SM	f_c=1kHz
Series switch	IGBT (two in series)
S_s switching frequency	f_h=10×f
Snubber resistance	200Ω
Snubber capacitance	1μF
RL load parameters	
Load resistance	R_{load}=13×f/50 Ω
Load inductance	L_{load}=2mH
PMSM parameters	
Rated active power	P=1.2MW
Number of pole pairs	pp=10
Rated rotor speed	n_{rated}=300r/min
Rated rms line-to-line voltage	U_{rated}=4kV
Mechanical load torque	T_{load}=34 000Nm

where U_{C1} and θ are the amplitude and phase angle, respectively, with

$$U_{C1}=\frac{I_{\text{OM}}}{4\omega_{\text{rated}}C}\sqrt{\begin{matrix}\left(1+m_{\text{rated}}\frac{\omega_{\text{rated}}-\omega}{\omega_{\text{rated}}}\right)^2+\frac{m_{\text{rated}}^4\cos^2\varphi}{4\omega_{\text{rated}}^2}\omega^2\\ -\frac{m_{\text{rated}}^2\cos^2\varphi}{\omega_{\text{rated}}}\left(1+m_{\text{rated}}\frac{\omega_{\text{rated}}-\omega}{\omega_{\text{rated}}}\right)\omega\end{matrix}} \tag{16}$$

$$\theta=\arctan\left(\frac{2\tan\varphi(\omega_{\text{rated}}+m_{\text{rated}}\omega_{\text{rated}}-m_{\text{rated}}\omega)}{(m_{\text{rated}}^2+2m_{\text{rated}})\omega-2\omega_{\text{rated}}-2m_{\text{rated}}\omega_{\text{rated}}}\right). \tag{17}$$

It is found that U_{C1} decreases as ω increases. (A detailed analysis is given in the Appendix.) Thus, the minimum capacitor voltage ripple occurs at rated speed and its amplitude is calculated by inserting $\omega=\omega_{\text{rated}}$ into (16), which is

$$U_{C1(\text{rated})}=\frac{I_{\text{OM}}}{8\omega_{\text{rated}}C}\sqrt{4+m_{\text{rated}}^4\cos^2\varphi-4m_{\text{rated}}^2\cos^2\varphi}. \tag{18}$$

On the other hand, the maximum capacitor voltage ripple is at zero speed, which can be derived by substituting $\omega=0$ into (16), that is

$$U_{C1(\text{zero})}=\frac{I_{\text{OM}}}{4\omega_{\text{rated}}C}(1+m_{\text{rated}}). \tag{19}$$

Hence, the maximum peak value of capacitor voltage is $U_{C(\text{rated})}+U_{C1(\text{zero})}$. This value cannot exceed the capacitor voltage limit U_{limit}, otherwise the capacitor may break down, which gives

$$U_{C(\text{rated})}+U_{C1(\text{zero})}\le U_{\text{limit}}. \tag{20}$$

According to (19), $U_{C1(zero)}$ is inversely proportional to the SM capacitance C. A larger C results in a smaller $U_{C(\text{rated})}+U_{C1(zero)}$. Therefore, to avoid overvoltage on the capacitor, the minimum capacitance for the HMMC can be determined by inserting (19) into (20), which gives

$$C_{\min\_1}=\frac{I_{\text{OM}}(1+m_{\text{rated}})}{4\omega_{\text{rated}}(U_{\text{limit}}-U_{C(\text{rated})})}. \tag{21}$$

This equation shows the dimension of the HMMC SM capacitance when the SM average capacitor voltage U_C keeps constant and is equal to $U_{C(\text{rated})}$.

III. AVERAGE CAPACITOR VOLTAGE DECREASE OPERATION OF THE HMMC

A. Selection of the SM Average Capacitor Voltage

For further reduction of the capacitance, an average capacitor voltage decrease operation of the HMMC is proposed. This operation decreases the SM average capacitor voltage U_C, so that a larger capacitor voltage ripple can be tolerated without overvoltage on the capacitor. In this case, U_C varies with output frequency and can be lower than $U_{C(\text{rated})}$. To maintain the arm output voltage, the arm insertion index of (10) needs to be modified

$$\begin{cases} n'_u=\frac{u_u}{NU_C}=\frac{U_{C(\text{rated})}}{U_C}n_u\\ n'_l=\frac{u_l}{NU_C}=\frac{U_{C(\text{rated})}}{U_C}n_l. \end{cases} \tag{22}$$

According to (11), (14), (15), and (22), the capacitor voltage ripple becomes

$$\begin{cases} \Delta u_{Cu}=\frac{U_{C(\text{rated})}}{U_C}U_{C1}\sin(\omega t+\theta)\\ \Delta u_{Cl}=-\frac{U_{C(\text{rated})}}{U_C}U_{C1}\sin(\omega t+\theta). \end{cases} \tag{23}$$

Then, the peak of capacitor voltage can be expressed as follows:

$$U_{C\_\text{peak}}=U_C+\frac{U_{C(\text{rated})}}{U_C}U_{C1}. \tag{24}$$

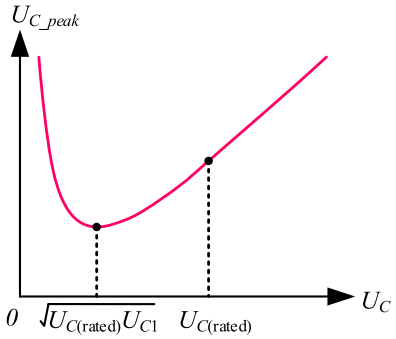

Fig. 3. Curve of relationship between U_{C_peak} and U_C.

This peak value should satisfy the constraint of

$$U_{C\_\text{peak}} \le U_{\text{limit}}. \tag{25}$$

Fig. 3 shows the relationship between U_{C_peak} and U_C. When U_C lies in $\left[\sqrt{U_{C(\text{rated})}U_{C1}}, U_{C(\text{rated})}\right]$, appropriately decreasing U_C can reduce U_{C_peak}. In order to find this desirable U_C, insert (24) into (25)

$$U_C^2 - U_{\text{limt}}U_C + U_{C(\text{rated})}U_{C1} \le 0 \tag{26}$$

which forms a quadratic equation of U_C. Before solving this equation, it is necessary to make sure real solutions exist. This means that the discriminant of the equation should satisfy $U_{\text{limit}}^2 - 4U_{C(\text{rated})}U_{C1} \ge 0$, which gives

$$U_{C1} \le \frac{U_{\text{limit}}^2}{4U_{C(\text{rated})}}. \tag{27}$$

With this constraint, U_C can be solved as follows:

$$U_{C\_a} \le U_C \le U_{C\_b} \tag{28}$$

where

$$\begin{cases} U_{C\_a} = \frac{U_{\text{limit}} - \sqrt{U_{\text{limit}}^2 - 4U_{C(\text{rated})}U_{C1}}}{2} \\ U_{C\_b} = \frac{U_{\text{limit}} + \sqrt{U_{\text{limit}}^2 - 4U_{C(\text{rated})}U_{C1}}}{2}. \end{cases} \tag{29}$$

In practice, to ensure sufficient output voltage in case of a sudden change of the motor load, the upper limit U_{C_b} is selected as the reference value of U_C

$$U_C = U_{C\_b}. \tag{30}$$

B. Dimensioning of the SM Capacitance

It should be noted that selection of U_C needs to ensure that the SM is not overmodulated, which means when $U_C = U_{C\_b}$, the sum of the capacitor voltages on each arm should be sufficient to support the arm output voltage. Since the upper and lower arms are symmetrical, taking upper arm as an example, that is

$$N(U_{C\_b} + \Delta u_{Cu}) \ge u_u + \Delta U. \tag{31}$$

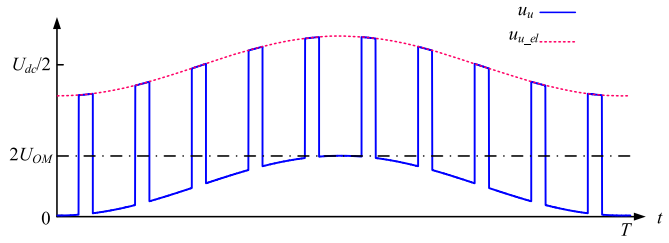

Fig. 4. Example of the HMMC up arm output voltage u_u and its envelope u_{u_el} in a cycle ($T = 2\pi/\omega$).

It is worth noting that a margin voltage ΔU is considered in (31). This voltage is used to provide circulating current control and accommodate any transient processes. Note that the arm voltage u_u is a switching waveform that is difficult to analyze. To simplify analysis, the envelope u_{u_el} is used, as shown in Fig. 4, and its expression is

$$u_{u\_el} = \frac{1}{2}NU_{C(\text{rated})}\left\{1 - \frac{m_{\text{rated}}}{\omega_{\text{rated}}}\omega\cos(\omega t)\right\}. \tag{32}$$

By replacing u_u in (31) with (32), we have

$$N(U_{C\_b} + \Delta u_{Cu}) \ge u_{u\_el} + \Delta U. \tag{33}$$

Then, inserting (23), (29), and (32) into (33) leads to

$$\begin{aligned} &N\left(\begin{array}{l}\frac{U_{\text{limit}} + \sqrt{U_{\text{limit}}^2 - 4U_{C(\text{rated})}U_{C1}}}{2} \\ + \frac{2U_{C(\text{rated})}}{U_{\text{limit}} + \sqrt{U_{\text{limit}}^2 - 4U_{C(\text{rated})}U_{C1}}}U_{C1}\sin(\omega t + \theta)\end{array}\right) \\ &\ge \tfrac{1}{2}NU_{C(\text{rated})}\left[1 - \tfrac{m_{\text{rated}}}{\omega_{\text{rated}}}\omega\cos(\omega t)\right] + \Delta U. \end{aligned} \tag{34}$$

Simplifying (34) gives

$$\begin{aligned} \sqrt{U_{\text{limit}}^2 - 4U_{C(\text{rated})}U_{C1}} &\ge \frac{1}{1 - \sin(\omega t + \theta)} \\ &\times \left\{\begin{array}{l}\left[1 - \frac{m_{\text{rated}}}{\omega_{\text{rated}}}\omega\cos(\omega t)\right]U_{C(\text{rated})} \\ + \frac{2\Delta U}{N} - [1 + \sin(\omega t + \theta)]\,U_{\text{limit}}\end{array}\right\}. \end{aligned} \tag{35}$$

It can be seen that the polynomial on the right-hand side of (35) varies cyclically with time t (whose cycle is $2\pi/\omega$). At any time, (35) must be satisfied to prevent overmodulation. Thus, $\sqrt{U_{\text{limit}}^2 - 4U_{C(\text{rated})}U_{C1}}$ has to be no less than the maximum of the right-hand side in (35). Define $u_m(\omega)$ as the maximum at angular frequency ω in a time cycle, which is expressed as Eq. (36). (Eq. (36) is shown on the bottom of this page.)

Then, the right-hand side of (35) can be replaced by $u_m(\omega)$, and (35) further becomes

$$U_{C1} \le \frac{U_{\text{limit}}^2 - u_m^2(\omega)}{4U_{C(\text{rated})}}. \tag{37}$$

$$u_m(\omega) = \max\left\{\left.\frac{\left(\begin{array}{l}\left[1 - \frac{m_{\text{rated}}}{\omega_{\text{rated}}}\omega\cos(\omega t)\right]U_{C(\text{rated})} \\ + \frac{2\Delta U}{N} - [1 + \sin(\omega t + \theta)]U_{\text{limit}}\end{array}\right)}{1 - \sin(\omega t + \theta)}\right| t \in \left[0, \frac{2\pi}{\omega}\right]\right\} \tag{36}$$

Hence, for any ω ($\omega \in [0, \omega_{\text{rated}}]$), (37) should be satisfied to avoid overmodulation when the average capacitor voltage U_C decreases to U_{C_b}. Moreover, this equation has a nice feature that it covers the constraint of (27). As such, when (37) is satisfied, the existence of the real solution U_{C_b} in (26) can be ensured.

According to (16), U_{C1} is inversely proportional to SM capacitance C. Thus, (37) also indicates how to dimension the capacitance. Substituting (16) into (37), the capacitance requirement is derived as follows:

$$C \geq \frac{I_{OM} U_{C(\text{rated})}}{\omega_{\text{rated}}} \times \frac{\sqrt{\left(1 + m_{\text{rated}} \frac{\omega_{\text{rated}} - \omega}{\omega_{\text{rated}}}\right)^2 + \frac{m_{\text{rated}}^4 \cos^2\varphi}{4\omega_{\text{rated}}^2}\omega^2} - \frac{m_{\text{rated}}^2 \cos^2\varphi}{\omega_{\text{rated}}}\left(1 + m_{\text{rated}} \frac{\omega_{\text{rated}} - \omega}{\omega_{\text{rated}}}\right)\omega}{U_{\text{limit}}^2 - u_m^2(\omega)}. \quad (38)$$

This equation varies with ω, which means different capacitances are required at different speeds. Hence, in order to cover the requirements of the capacitance within the whole speed range, the minimum SM capacitance can be determined by the maximum value of (38) with $\omega \in [0, \omega_{\text{rated}}]$

$$C_{\text{min\_2}} = \frac{I_{\text{OM}} U_{C(\text{rated})} \chi}{\omega_{\text{rated}}} \quad (39)$$

where eq. 40 as shown bottom of the page.

It should be noted that the calculations of $u_m(\omega)$ and χ are very complex, which has to be solved by the aid of numerical solution.

Therefore, under this average capacitor voltage decrease operation, the SM capacitance can be dimensioned by (39). While in the traditional operation whose average capacitor voltage is constant, the SM capacitance needs to be determined as (21). Fig. 5 further shows an example of the SM capacitance under different capacitor peak voltage limits U_{limit}. The HMMC parameters of this example are as follows: $m_{\text{rated}} = 0.8$, $\cos\varphi = 0.99$, and $\Delta U = 11\%\, U_{\text{dc}}$. It can be seen that at the same capacitor peak voltage limit, in contrast to the traditional operation, the required SM capacitance is greatly reduced with the proposed operation. When U_{limit} is above 120% $U_{C(\text{rated})}$, the effectiveness of the proposed method is weakened. This is because a high U_{limit} allows a large capacitor voltage ripple, and the converter already has enough capacitance in this case.

IV. Simulation and Experimental Results

A. Simulation Results With RL Loads

In order to verify the effectiveness of the proposed method, a 1.2-MW HMMC is simulated, using MATLAB /Simulink software. The HMMC is designed with ten SMs per arm, and the rated capacitor voltage is 800 V. Detailed parameters of the

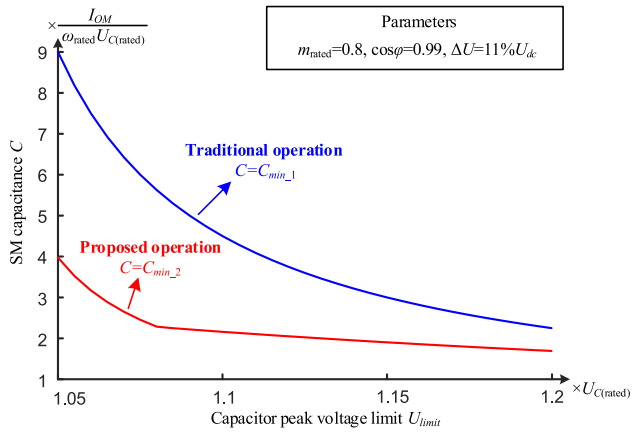

Fig. 5. Example of the SM capacitance dimensioning of traditional and proposed operations in dependence of the capacitor peak voltage limit.

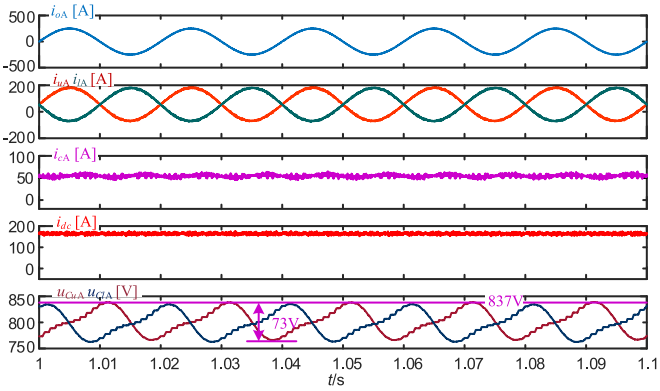

Fig. 6. Simulation waveforms of the HMMC at 50 Hz.

simulated circuit and operating conditions are listed in Table I. The *RL* load is used to test the steady-state performance. The load resistance varies linearly with the output frequency ($R_{\text{load}} = 13 \times f50\,[\Omega]$) to emulate the constant torque characterisitc (with $I_{\text{OM}} = 250$ A) of the motor. According to the line of proposed operation shown in Fig. 5, the SM capacitance is selected as 4 mF with the capacitor peak voltage limit U_{limit} set to 840 V ($1.05U_{C(\text{rated})}$).

Fig. 6 shows the operation waveforms of the HMMC at a rated frequency ($f_{\text{rated}} = 50$ Hz). The HMMC operates as the traditional MMC with the series switch kept ON. The dc current i_{dc} is at its rated value 150 A, and the arm current ($i_{u\text{A}}$ and $i_{l\text{A}}$) amplitudes are approximately 175 A, which equals ($1/3I_{\text{dc}} + 1/2I_{\text{OM}}$). Average capacitor voltage U_C is equal to $U_{C(\text{rated})}$ (800 V), and the peak value of capacitor voltage U_{C_peak} is 837 V. It is worth to note that the series switch is constantly ON and generates additional conduction loss at the rated frequency. To compare the losses, the 1.2-MW MMC in the simulation study (parameters are shown in Table I, and the Infineon

$$\chi = \max\left\{ \left| \frac{\sqrt{\left(1 + m_{\text{rated}} \frac{\omega_{\text{rated}} - \omega}{\omega_{\text{rated}}}\right)^2 + \frac{m_{\text{rated}}^4 \cos^2\varphi}{4\omega_{\text{rated}}^2}\omega^2} - \frac{m_{\text{rated}}^2 \cos^2\varphi}{\omega_{\text{rated}}}\left(1 + m_{\text{rated}} \frac{\omega_{\text{rated}} - \omega}{\omega_{\text{rated}}}\right)\omega}{U_{\text{limit}}^2 - u_m^2(\omega)} \right| \omega \in [0, \omega_{\text{rated}}] \right\} \quad (40)$$

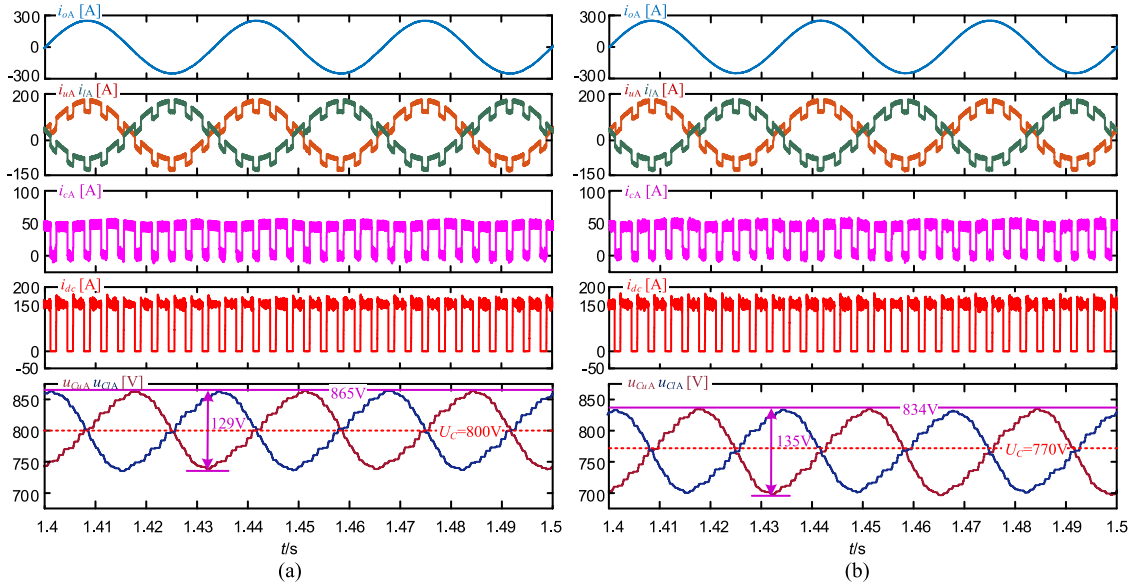

Fig. 7. Simulation waveforms of the HMMC at 30 Hz. (a) Traditional operation (U_C = 800 V). (b) Proposed operation (U_C = 770 V).

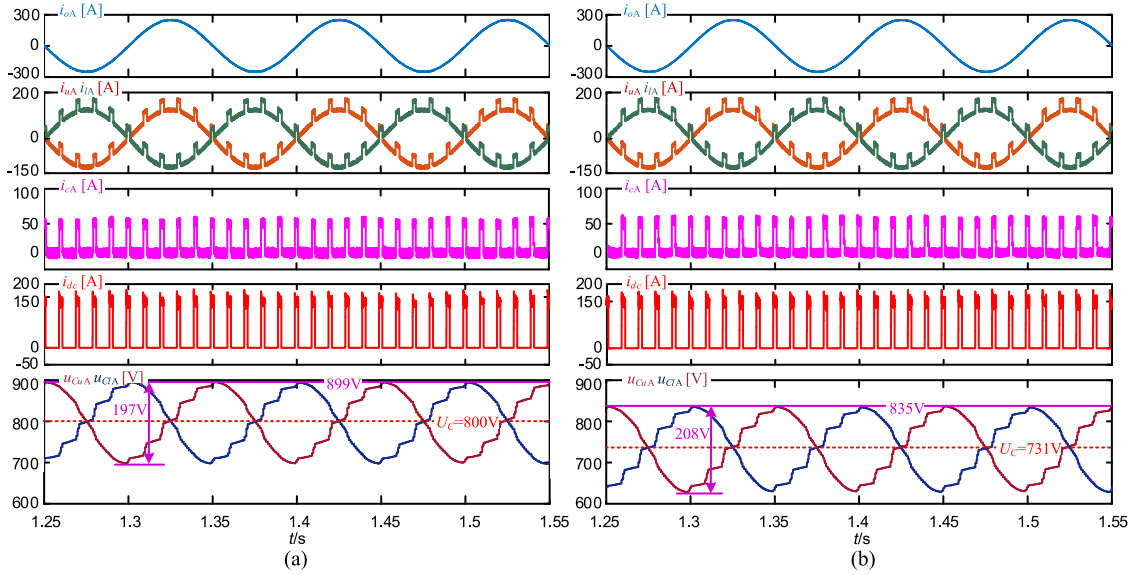

Fig. 8. Simulation waveforms of the HMMC at 10 Hz. (a) Traditional operation (U_C = 800 V). (b) Proposed operation (U_C = 731 V).

FZ600R12KE3 IGBTs are adopted in the SMs) is analyzed, which presents an efficiency of 99.35% at the rated frequency. Then, conduction loss of the series switch (including three Infineon FZ400R33KL2C_B5 IGBTs) is estimated as 0.95 kW, and the efficiency of HMMC is 99.27%. The losses are increased by approximately 12%, which is acceptable. Moreover, a bypass switch can be used to bypass the series switch when the HMMC is at the rated frequency, to further reduce this loss.

In the proposed average capacitor voltage decreasing operation, U_C is selected as the reference U_{C_b} in (29). Fig. 7(a) and (b) shows the simulation waveforms of the HMMC at 30 Hz under the traditional and proposed operations, respectvely. In Fig. 7(a), U_{C_peak} is 865 V, which exceeds the capacitor peak voltage limit (U_{limit} = 840 V). While decreasing U_C from 800 to 770 V, U_{C_peak} is 834 V, as shown in Fig. 7(b). When frequency f decreases to 10 Hz, U_{C_peak} rises to 899 V, as shown in Fig. 8(a). But, with U_C reduced to 731 V, U_{C_peak} is only 835 V, as shown in Fig. 8(b). These confirm the proposed operation has lower peak of the capacitor voltage.

Fig. 9(a) and (b) further shows the simulation waveforms of HMMC at 2 Hz. Under this very low frequency, U_{C_peak} increases dramatically to 917 V, as shown in Fig. 9(a). In contrast, U_{C_peak} is still 837 V by decreasing U_C to 708 V, as shown in Fig. 9(b). This proves that the proposed operation can still effectively reduce the peak value of capacitor voltage even at very low frequencies.

To show that the reduction of U_C does not result in overmodulation, the simulation waveforms of the inserted arm voltage at 50 Hz, 30 Hz, and 2 Hz are shown in Figs. 10–12, respectively. It is shown that summation of the capacitor voltage $\Sigma u_{Cu\text{A}}$ is

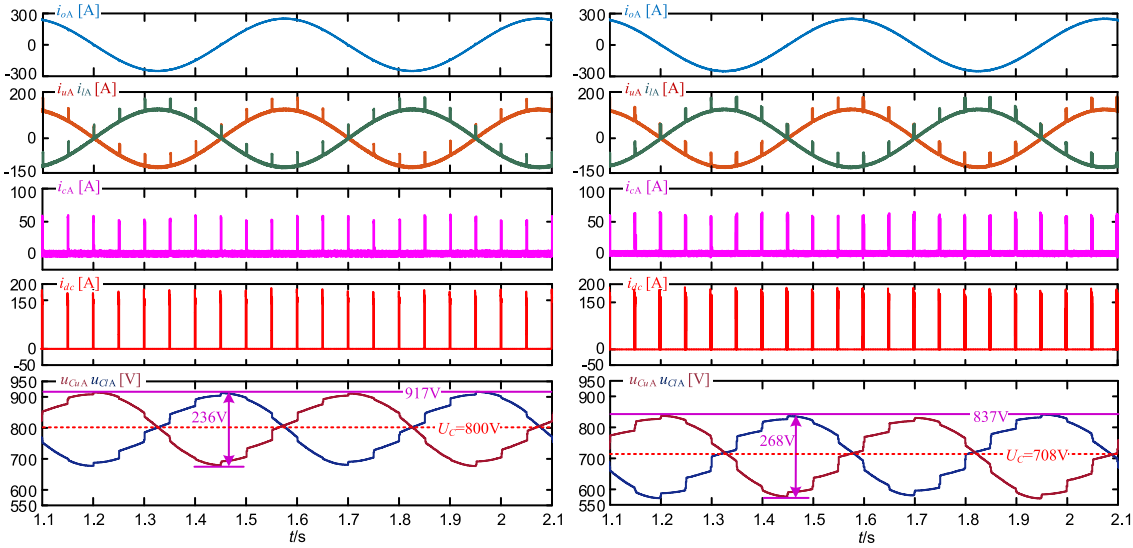

Fig. 9. Simulation waveforms of the HMMC at 2 Hz. (a) Traditional operation ($U_C = 800$ V). (b) Proposed operation ($U_C = 708$ V).

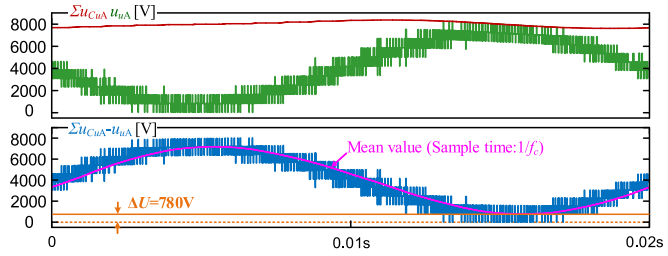

Fig. 10. Sum capacitor voltage and inserted voltage of the upper arm with the proposed method at 50 Hz.

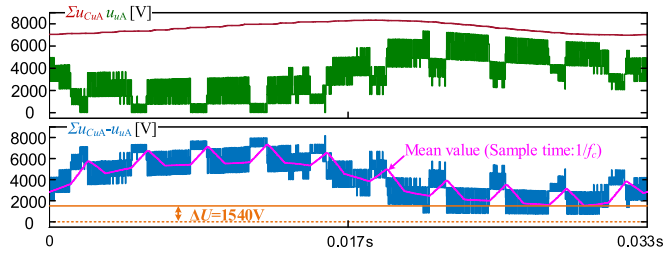

Fig. 11. Sum capacitor voltage and inserted voltage of the upper arm with the proposed method at 30 Hz.

always higher than the inserted arm voltage $u_{u\mathrm{A}}$, with a minimum voltage margin of $\Sigma u_{C\,u\mathrm{A}} - u_{u\mathrm{A}} = 780$ V. The theoretical voltage margin is designed as 880 V, so there is an 11% deviation between the theoretical and actual values. This is because the voltage drop across the arm inductor and the second-order harmonic component of the capacitor voltage are ignored for simplicity in the analysis.

A detailed comparison of the simulation results at different frequencies is illustrated in Fig. 13. It can be seen that in the traditional operation, U_C remains constant; thus, $U_{C\,\text{-peak}}$ increases when the frequency decreases and its maximum is up to 917 V. This maximum peak is far more than the capacitor peak voltage limit ($U_{\text{limit}} = 840$ V), which means a larger capacitance is needed. However, the proposed operation reduces U_C as the

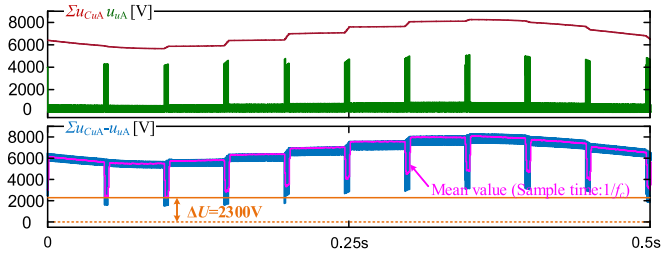

Fig. 12. Sum capacitor voltage and inserted voltage of the upper arm with the proposed method at 2 Hz.

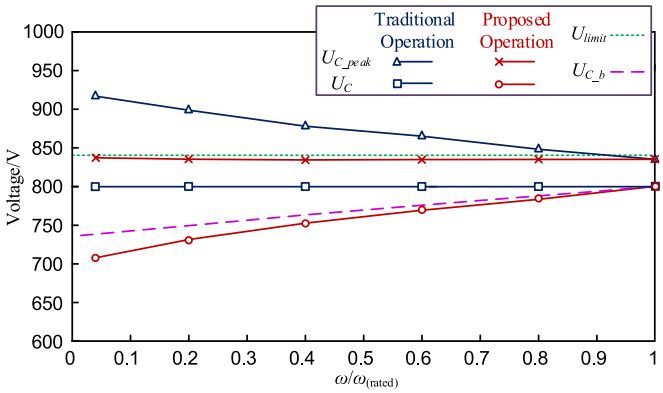

Fig. 13. Comparison of the simulation results in full frequency ranges.

frequency decreases, and $U_{C\,\text{-peak}}$ is stable at only 837 V within the whole frequency range. So, the capacitance does not need to be increased. In other words, under the same capacitor peak voltage limit, the proposed operation can reduce the capacitance significantly.

B. Simulation Results With PMSM

To test the dynamic performance of the proposed method at a low frequency, a 1.2-MW/4-kV permanent magnet synchronous motor (PMSM) startup is simulated (detailed

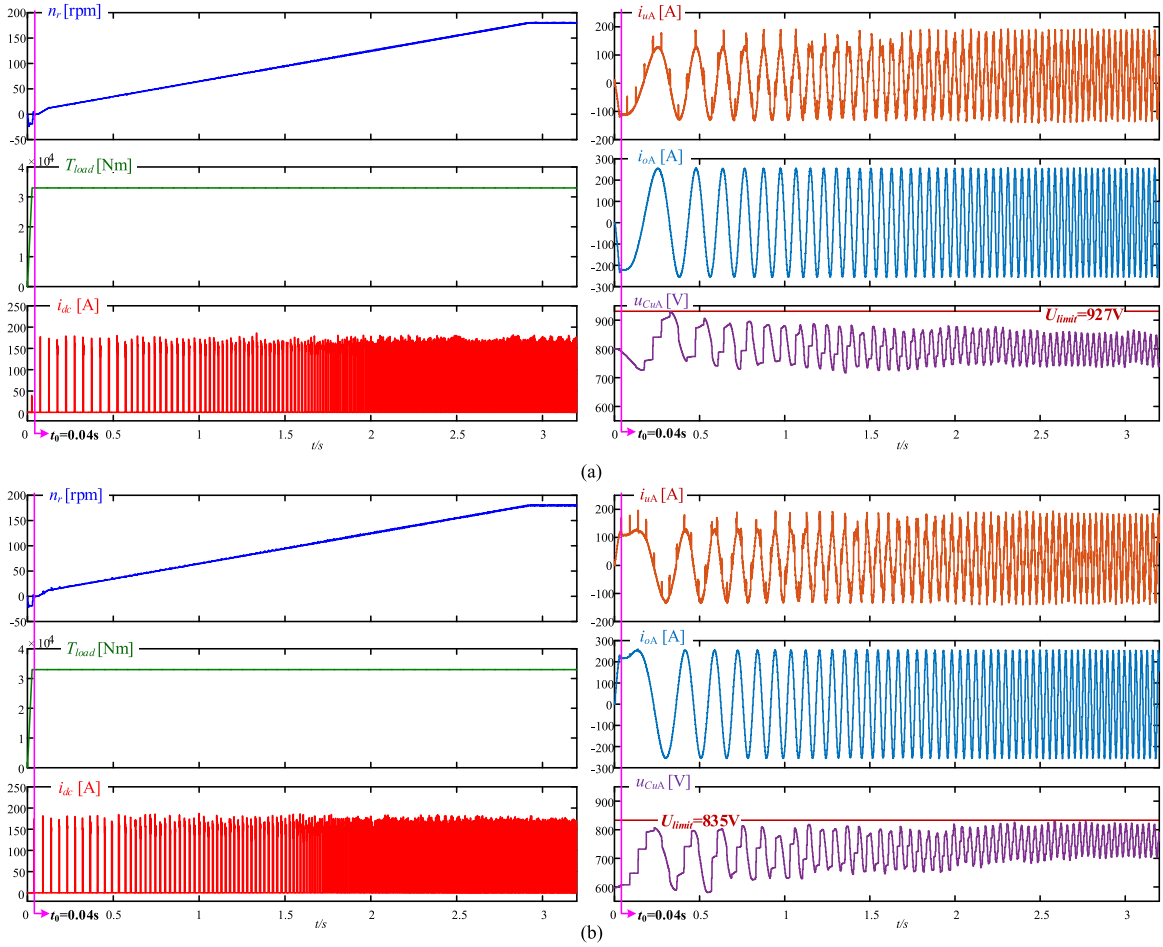

Fig. 14. Simulation waveforms of a PMSM motor driven by the HMMC from standstill to 180 r/min with constant load torque. (a) Traditional operation. (b) Proposed operation.

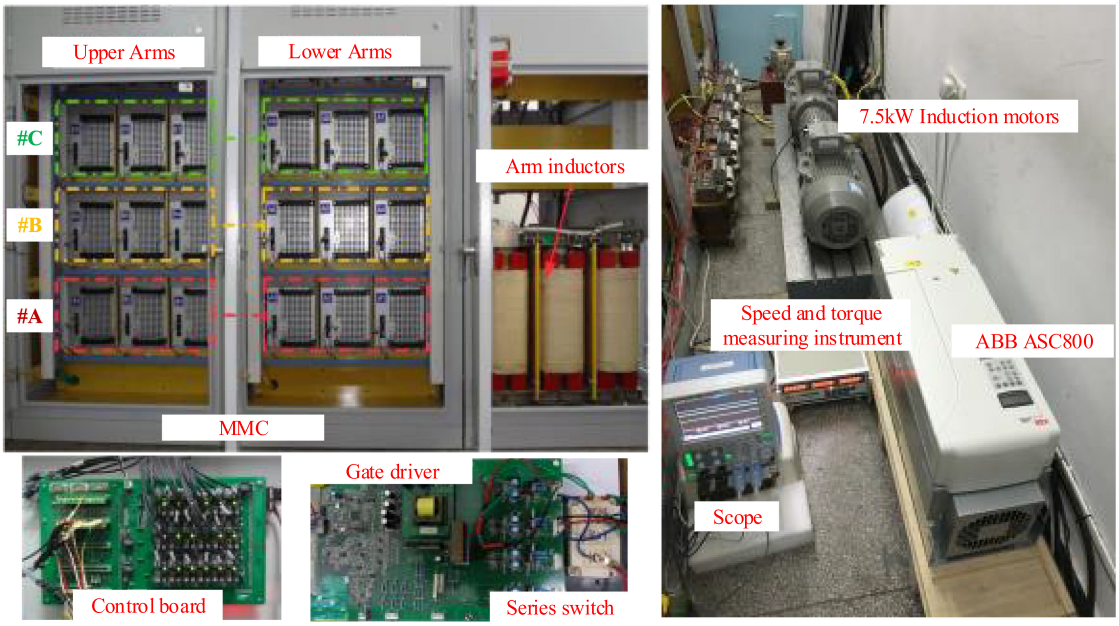

Fig. 15. Pictures of the HMMC motor drive platform.

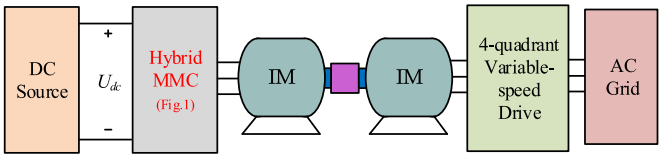

Fig. 16. Experimental circuit configuration.

TABLE II
EXPERIMENTAL PARAMETERS

HMMC parameters	
Number of SMs per arm	N=3
DC-source voltage	U_{dc}=450V
Rated SM average capacitor voltage	U_{CN}=150V
Margin voltage	ΔU=78V
SM capacitor peak voltage limit	U_{limit}=164V
SM capacitance	C=1.86mF
Arm inductance	L=2mH
Rated output frequency	f_{rated}=30Hz
Rated modulation index	m_N=0.8
Rated phase current amplitude	$I_{OM(\text{rated})}$=15A
Rated dc current	$I_{dc(\text{rated})}$=8A
PSC-PWM frequency	f_c=3kHz
Series switch	IGBT(FF300R12KE3)
S_s switching frequency	f_h=10×f
Snubber resistance	37Ω
Snubber capacitance	10μF
IM parameters	
Rated power	S=7.5kw
Number of poles	p=2
Rated speed	n_r=1460rpm
Stator line-line rated rms voltage	U_l=380V
Stator line-line rated rms voltage	I_l=15.7A
Power factor	cosφ=0.82

parameters are shown in Table I). As shown in Fig. 14(a), starting from 0.04 s ($t_0 = 0.04$ s), the PMSM accelerates from standstill to 180 r/min with constant torque. The maximum U_{C_peak} is 927 V, which is severely out of the capacitor peak voltage limit U_{limit} (840 V). So, a larger capacitance is needed. Under the same simulation conditions, for the proposed method, as shown in Fig. 14(b), the maximum U_{C_peak} is below U_{limit} (which is only 835 V). Thus, the proposed method can realize low-speed operation without increasing the SM capacitance.

C. Experimental Results With Induction Motor (IM)

The proposed operation is further verified by a scaled-down HMMC motor drive platform, as shown in Figs. 15 and 16. There are two IMs (Siemens 1LE0001-1CB23-3AA4). One is driven by a four quadrant drive (ABB ASC800-11-0016-3) providing a constant torque load. The other is driven by the HMMC, which contains three SMs per arm with the rated average capacitor voltage of 150 V. Detailed parameters of the experimental platform are listed in Table II.

Due to limitation of the prototype, the maximum output voltage of the HMMC cannot satisfy the full magnetization voltage that IM requires at the rated speed. Thereby the base speed here

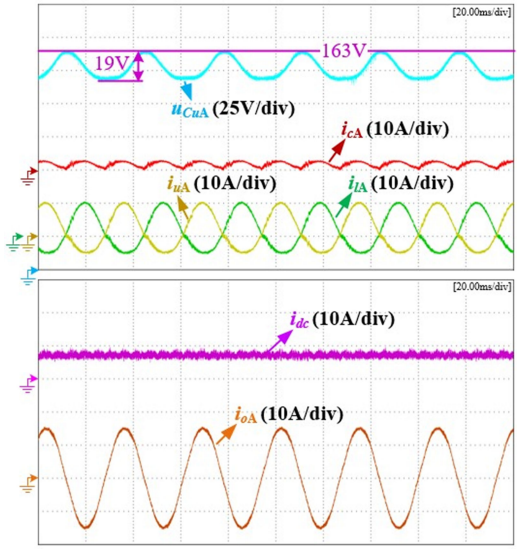

Fig. 17. Experimental waveforms of the HMMC at 30 Hz.

is set to 60% of IM rated speed, i.e., $f_{\text{rated}} = 30$ Hz. The motor load torque is constant, which is 25 N·m with I_{OM} being 15 A. In the experiment, U_{limit} is set to 164 V ($1.09U_{C(\text{rated})}$). According to (39), the SM capacitance is selected as 1.86 mF.

Fig. 17 shows the experimental results of HMMC at the rated frequency $f = 30$ Hz. The waveforms are the same as the traditional MMC, where the dc current i_{dc} is at its rated value 8 A and the arm currents ($i_{u\text{A}}$ and $i_{l\text{A}}$) amplitudes are about 10 A. The peak value of capacitor voltage U_{C_peak} is 163 V with the capacitor voltage ripple of 19 V.

Fig. 18(a) and (b) compares the waveforms in the traditional and proposed operations at 20 Hz. In Fig. 18(a), U_C is equal to its rated value 150 V and U_{C_peak} is 166 V. When decreasing U_C to 145 V, U_{C_peak} is reduced to 160 V, as shown in Fig. 18(b). When the HMMC operates at 15 Hz, U_{C_peak} is 168 V, as shown in Fig. 19(a), and it is suppressed to 160 V with the decrease of U_C, as shown in Fig. 19(b). As f is further reduced to 10 Hz, U_{C_peak} rises to 171 V, as shown in Fig. 20(a). With decreasing U_C from 150 to 134 V, U_{C_peak} is only 161 V, as shown in Fig. 20(b).

When the HMMC operates at low frequency $f = 5$ Hz, as shown in Fig. 21(a), the capacitor voltage ripple becomes large (58 V), leading to a very high peak $U_{C\_\text{peak}} = 181$ V. This has been out of the capacitor peak voltage limit U_{limit} (164 V). But in Fig. 21(b), by decreasing U_C to 127 V, a larger capacitor voltage ripple (69 V) can be tolerated and U_{C_peak} is only 162 V.

Fig. 22 shows the experimental waveforms of S_s with the proposed method at 5 Hz. Before S_s is turned OFF, i_{dc} is already brought to zero. The voltage of the series switch u_{ss} has very little voltage spike (about 15 V) during switching OFF process, of which peak value is about 380 V.

Fig. 23(a) and (b) further shows the experimental results at 3 Hz. Under this very low frequency, the proposed operation can still maintain U_{C_peak} at 164 V, as shown in Fig. 23(b), where U_{C_peak} is reduced by 20 V compared with Fig. 23(a). It verifies

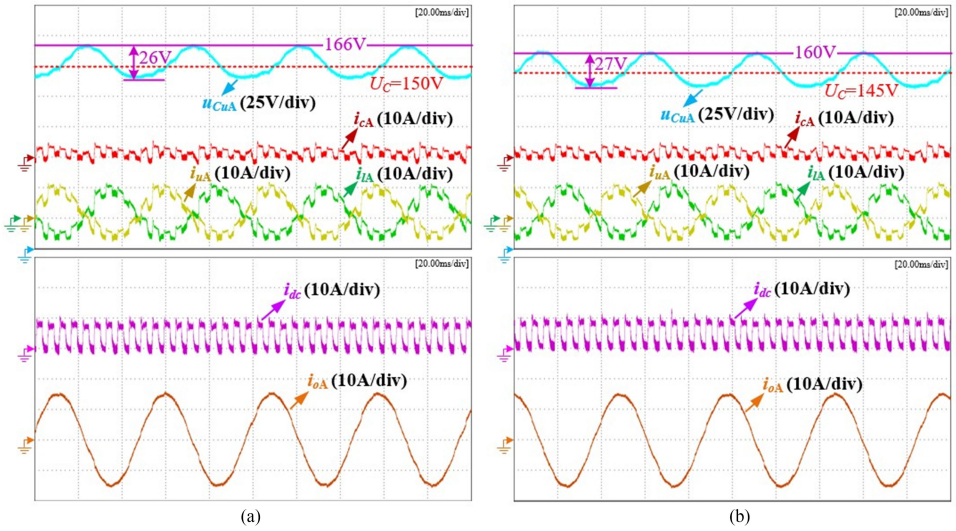

Fig. 18. Experimental waveforms of the HMMC at 20 Hz. (a) Traditional operation ($U_C = 150$ V). (b) Proposed operation ($U_C = 145$ V).

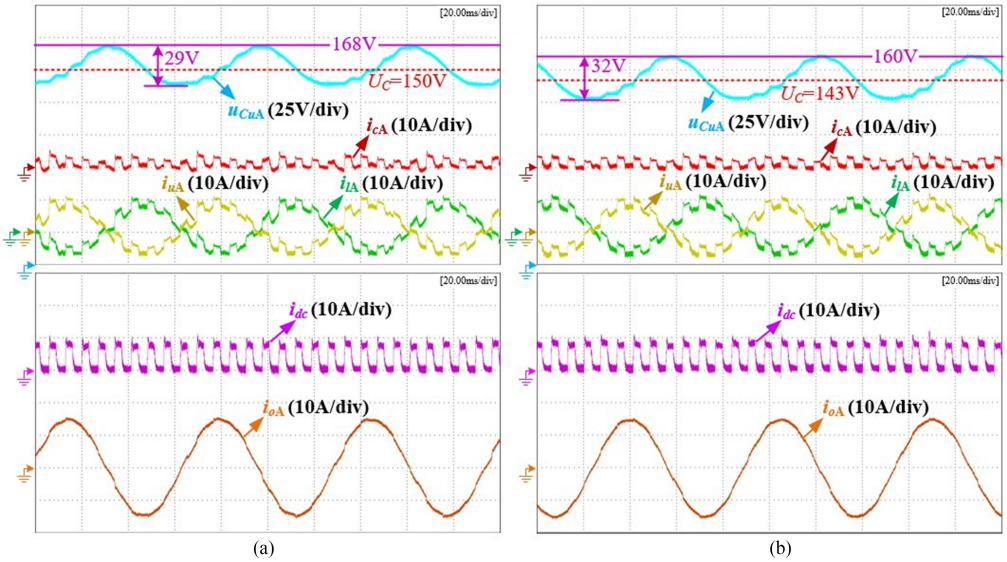

Fig. 19. Experimental waveforms of the HMMC at 15 Hz. (a) Traditional operation ($U_C = 150$ V). (b) Proposed operation ($U_C = 143$ V).

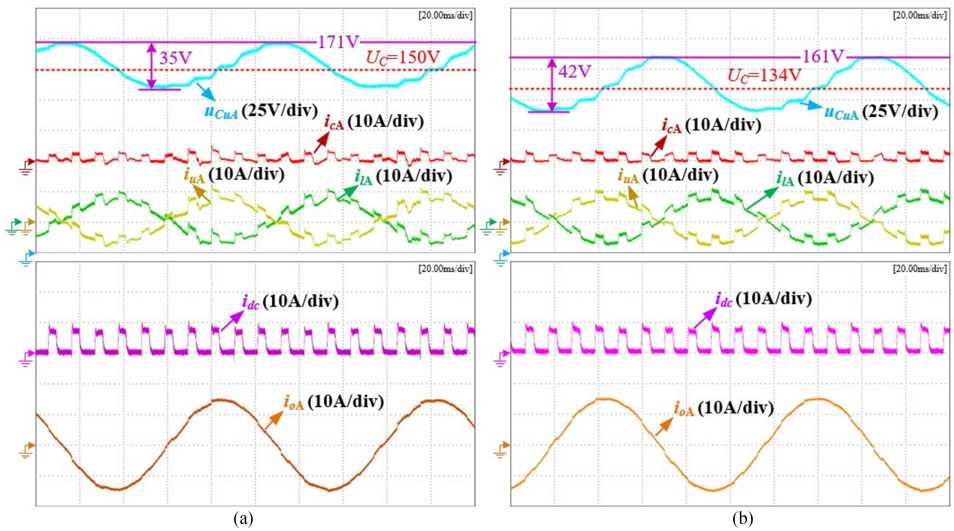

Fig. 20. Experimental waveforms of the HMMC at 10 Hz. (a) Traditional operation ($U_C = 150$ V). (b) Proposed operation ($U_C = 134$ V).

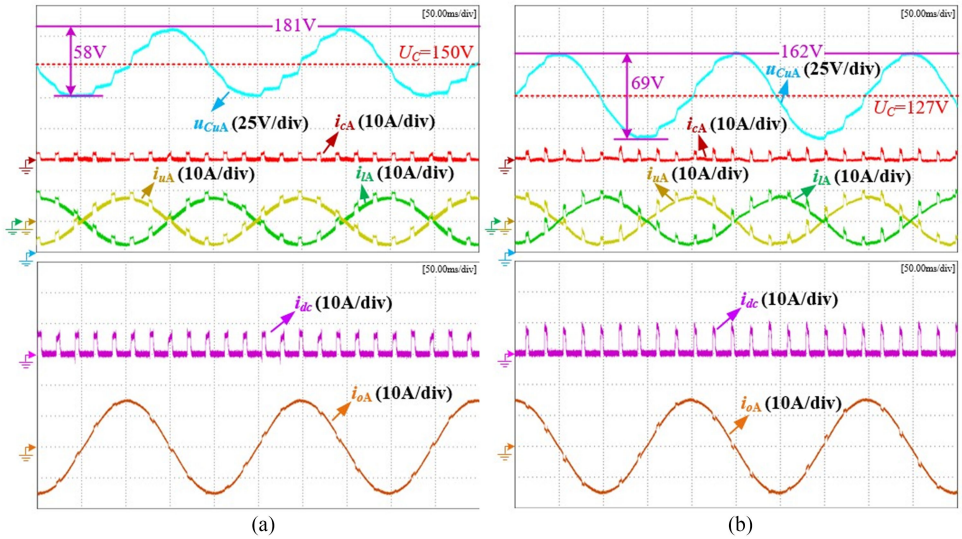

Fig. 21. Experimental waveforms of the HMMC at 5 Hz. (a) Traditional operation (U_C = 150 V). (b) Proposed operation (U_C = 127 V).

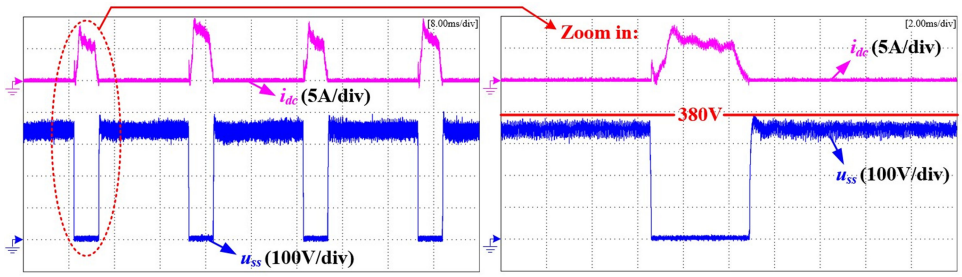

Fig. 22. Experimental waveforms of series switch of the HMMC with the proposed method at 5 Hz.

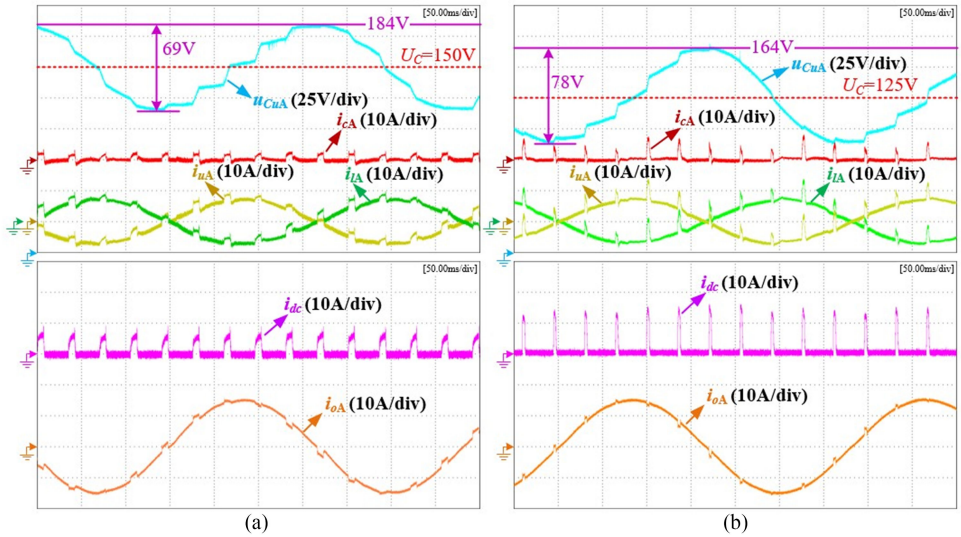

Fig. 23. Experimental waveforms of the HMMC at 3 Hz. (a) Traditional operation (U_C = 150 V). (b) Proposed operation (U_C = 125 V).

that the proposed operation can effectively reduce the peak of capacitor voltage within the whole frequency range.

Fig. 24 summaries the experimental results. In the traditional operation, U_C is constant and U_{C_peak} increases as the frequency decreases. The maximum of U_{C_peak} is 184 V, which exceeds the capacitor peak voltage limit (U_{limit} = 164 V) by a great deal, indicating a larger capacitance is needed to limit U_{C_peak}. But for the proposed operation, U_C decreases with the reduction of frequency, making U_{C_peak} remain around 163 V within the whole frequency range. This means the proposed operation results in a significant reduction of the capacitance under the same capacitor peak voltage limit. It should be noted that the

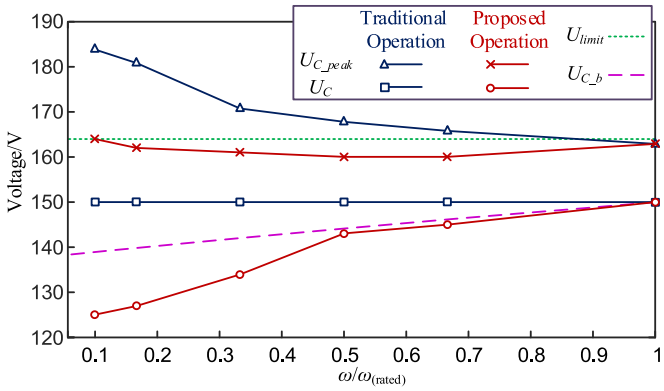

Fig. 24. Comparison of the experimental results in full frequency ranges.

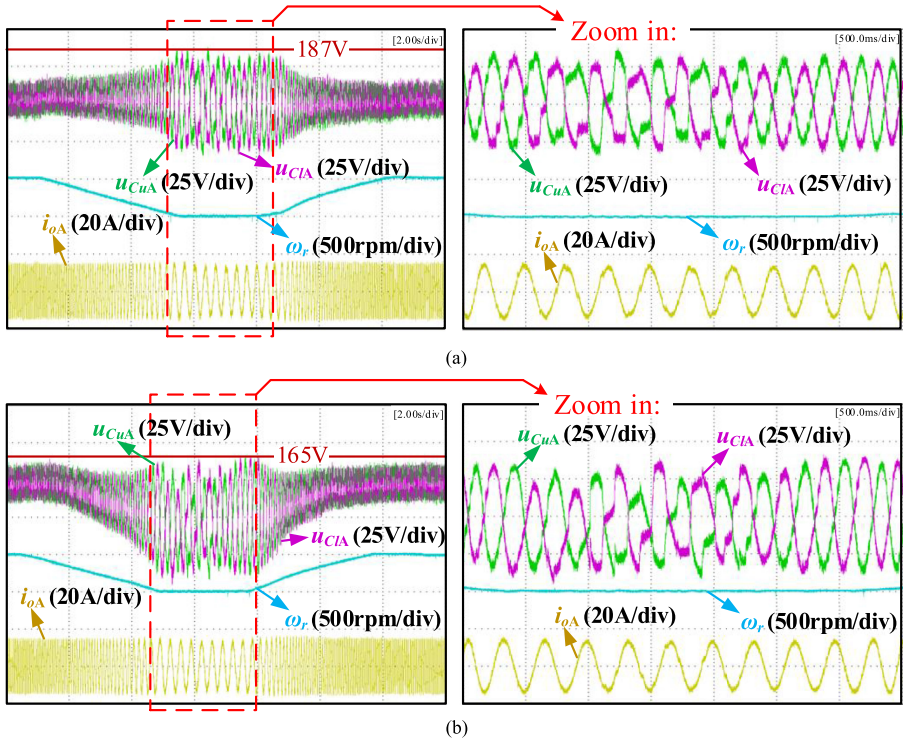

Fig. 25. Acceleration/deceleration experimental waveforms of an IM motor driven by the HMMC. (a) Traditional operation. (b) Proposed operation.

experimental value U_C is lower than its reference U_{C_b}, particularly at low frequencies. This is due to the nonlinearity of the motor volt/hertz ratio at low frequencies, which means amplitude U_{OM} has to be increased to compensate the voltage drop of the motor stator. Thus, the dc voltage seen by the HMMC u_d in (7) also needs to be increased, leading to the increase of the capacitor ripple and U_{C_peak}. Hence, a lower U_C has to be used.

Fig. 25(a) further shows the IM acceleration/deceleration experimental waveforms with the traditional operation. The motor decelerates from 500 r/min to zero speed and maintains about 2.5 s. Then, the motor accelerates from zero speed back to 500 r/min. The torque is kept constant throughout the acceleration/deceleration process and the magnitude of output current $i_{o\mathrm{A}}$ keeps 15 A. The maximum of U_{C_peak} is 187 V. Under the same experimental conditions, with the proposed method the maximum of U_{C_peak} is further reduced to 167 V, as shown in Fig. 25(b). Thus, the effectiveness of the proposed method is also verified.

It is worth to note that at speeds very close to zero (below 1–2 Hz), the duty cycle D of the HMMC will be so small that it approaches the time limit for current control, and the SM capacitor voltage ripple will be much larger. Therefore, it is not possible for the HMMC to drive a motor stably operating at zero speed with a high torque request [22]. However, most of the industrial motors are not required to stably operate at zero speed, despite starting torque is always required to overcome the initial friction. It is naturally easy for the HMMC to surpass the very-close-to-zero speed region due to the acceleration of the motors,

and the SM capacitor voltage ripple would be reasonably limited (as shown in Fig. 14). Moreover, for IM, existence of the slip makes the frequency of the stator higher than the rotor. Hence, when the rotor is at zero speed, frequency of the stator current is not zero, and the HMMC can even stably operate at zero speed (as shown in Fig. 25).

V. Conclusion

HMMC is a promising topology for MV variable-speed drives, due to its distinctive features, such as lower capacitor voltage ripple, high efficiency, and no common-voltage problem. In this paper, to further reduce the capacitance of the HMMC, the average capacitor voltage decrease operation is proposed. The peak of capacitor voltage can be reduced and a larger capacitor voltage ripple can be tolerated even at very low speed. Selection of the average capacitor voltage is presented, and dimensioning of the SM capacitance is also discussed. The feasibility and effectiveness of the proposed method are confirmed by simulation and experimental results.

Appendix: Proof of the Capacitor Voltage Ripple Monotonicity

In (16), to prove that U_{C1} is reduced with the increase of ω, the first derivative of U_{C1} versus ω is analyzed

$$\frac{dU_{C1}}{d\omega} = \frac{I_{\mathrm{OM}}}{8\omega_{\mathrm{rated}} C\sqrt{\mu}} \frac{d\mu}{d\omega} \tag{A1}$$

where

$$\mu = \left(1 + m_{\mathrm{rated}} \frac{\omega_{\mathrm{rated}} - \omega}{\omega_{\mathrm{rated}}}\right)^2 + \frac{m_{\mathrm{rated}}^4 \cos^2\varphi}{4\omega_{\mathrm{rated}}^2}\omega^2 - \frac{m_{\mathrm{rated}}^2 \cos^2\varphi}{\omega_{\mathrm{rated}}} \left(1 + m_{\mathrm{rated}} \frac{\omega_{\mathrm{rated}} - \omega}{\omega_{\mathrm{rated}}}\right)\omega. \tag{A2}$$

In motor drive applications, a constant m/ω ratio (i.e., volt/hertz ratio) and I_{OM} is ensured, and the power factor $\cos\varphi$ is basically constant. Then, $d\mu/d\omega$ can be derived as follows:

$$\frac{d\mu}{d\omega} = \frac{0.5m_{\mathrm{rated}}^4 \cos^2\varphi + m_{\mathrm{rated}}^3 \cos^2\varphi}{\omega_{\mathrm{rated}}} \frac{\omega}{\omega_{\mathrm{rated}}} - \left(\frac{2m_{\mathrm{rated}} + m_{\mathrm{rated}} \cos^2\varphi}{\omega_{\mathrm{rated}}}\right)\left(1 - m_{\mathrm{rated}} \frac{\omega_{\mathrm{rated}} - \omega}{\omega_{\mathrm{rated}}}\right). \tag{A3}$$

When ω is $0\sim\omega_{\mathrm{rated}}$, the following expressions are satisfied:

$$\frac{\omega}{\omega_{\mathrm{rated}}} \le 1 \tag{A4}$$

$$1 + m_{\mathrm{rated}} \frac{\omega_{\mathrm{rated}} - \omega}{\omega_{\mathrm{rated}}} \ge 1. \tag{A5}$$

Inserting (A4) and (A5) into (A3), gives

$$\frac{d\mu}{d\omega} \le \frac{0.5m_{\mathrm{rated}}^4 \cos^2\varphi + m_{\mathrm{rated}}^3 \cos^2\varphi}{\omega_{\mathrm{rated}}} - \frac{2m_{\mathrm{rated}} + m_{\mathrm{rated}} \cos^2\varphi}{\omega_{\mathrm{rated}}}. \tag{A6}$$

Note that

$$\frac{0.5m_{\mathrm{rated}}^4 \cos^2\varphi + m_{\mathrm{rated}}^3 \cos^2\varphi}{\omega_{\mathrm{rated}}} - \frac{2m_{\mathrm{rated}} + m_{\mathrm{rated}} \cos^2\varphi}{\omega_{\mathrm{rated}}} = -\frac{m_{\mathrm{rated}}}{\omega_{\mathrm{rated}}} \left\{(2 - 0.5m_{\mathrm{rated}}^3 \cos^2\varphi) + \cos^2\varphi(1 - m_{\mathrm{rated}}^2)\right\} \tag{A7}$$

and

$$2 - 0.5m_{\mathrm{rated}}^3 \cos^2\varphi > 0, \quad \cos^2\varphi(1 - m_{\mathrm{rated}}^2) \ge 0 \tag{A8}$$

with the absolute values of m_{rated} and $\cos\varphi$ no higher than 1. Inserting (A6)–(A8) into (A1), it can be obtained that

$$\frac{dU_{C1}}{d\omega} < 0. \tag{A9}$$

Hence, U_{C1} is monotonously decreasing as ω increases. This means U_{C1} reaches the minimum and maximum values when $\omega = \omega_{\mathrm{rated}}$ and $\omega = 0$, respectively, as shown in (18) and (19).

References

[1] M. Hagiwara, K. Nishimura, and H. Akagi, "A medium-voltage motor drive with a modular multilevel PWM inverter," *IEEE Trans. Power Electron.*, vol. 25, no. 7, pp. 1786–1799, Jul. 2010.

[2] M. A. Perez, S. Bernet, J. Rodriguez, S. Kouro, and R. Lizana, "Circuit topologies, modeling, control schemes, and applications of modular multilevel converters," *IEEE Trans. Power Electron.*, vol. 30, no. 1, pp. 4–14, Jan. 2015.

[3] S. Debnath, J. Qin, B. Bahrani, M. Saeedifard, and P. Barbosa, "Operation, control, and applications of the modular multilevel converter: A review," *IEEE Trans. Power Electron.*, vol. 30, no. 1, pp. 37–53, Jan. 2015.

[4] G. J. M. de Sousa and M. L. Heldwein, "Modular multilevel converter based unidirectional medium/high voltage drive system," in *Proc. 39th Annu. Conf. IEEE Ind. Electron. Soc.*, 2013, pp. 1037–1042.

[5] M. Hiller, D. Krug, R. Sommer, and S. Rohner, "A new highly modular medium voltage converter topology for industrial drive applications," in *Proc. 13th Eur. Conf. Power Electron. Appl.*, Barcelona, Spain, 2009, pp. 1–10.

[6] A. Antonopoulos, L. Angquist, S. Norrga, K. Ilves, L. Harnefors, and H.-P. Nee, "Modular multilevel converter ac motor drives with constant torque from zero to nominal speed," *IEEE Trans. Ind. Appl.*, vol. 50, no. 3, pp. 1982–1993, May/Jun. 2014.

[7] A. Antonopoulos, L. Angquist, L. Harnefors, and H.-P. Nee, "Optimal selection of the average capacitor voltage for variable-speed drives with modular multilevel converters," *IEEE Trans. Power Electron.*, vol. 30, no. 1, pp. 227–234, Jan. 2015.

[8] A. Korn, M. Winkelnkemper, and P. Steimer, "Low output frequency operation of the modular multi-level converter," in *Proc. IEEE Energy Convers. Congr. Expo.*, 2010, pp. 3993–3997.

[9] M. Spichartz, V. Staudt, and A. Steimel, "Modular multilevel converter for propulsion system of electric ships," in *Proc. IEEE Elect. Ship Technol. Symp.*, 2013, pp. 237–242.

[10] M. Hagiwara, I. Hasegawa, and H. Akagi, "Start-up and low-speed operation of an electric motor driven by a modular multilevel cascade inverter," *IEEE Trans. Ind. Appl.*, vol. 49, no. 4, pp. 1556–1565, Jul./Aug. 2013.

[11] J. Jung, H. Lee, and S.-K. Sul, "Control strategy for improved dynamic performance of variable-speed drives with modular multilevel converter," *IEEE J. Emerg. Sel. Topics Power Electron.*, vol. 3, no. 2, pp. 371–380, Jun. 2015.

[12] L. He, K. Zhang, J. Xiong, S. Fan, and Y. Xue, "Low-frequency ripple suppression for medium-voltage dives using modular multilevel converter with full-bridge submodules," *IEEE J. Emerg. Sel. Topics Power Electron.*, vol. 4, no. 2, pp. 657–667, Jun. 2016.

[13] B. Li *et al.*, "An improved circulating current injection method for modular multilevel converter in variable-speed drives," *IEEE Trans. Ind. Electron.*, vol. 63, no. 11, pp. 7215–7225, Nov. 2016.

[14] B. Li, S. Zhou, D. Xu, D. Xu, and W. Wang, "Comparative study of the sinusoidal-wave and square-wave circulating current injection methods for low-frequency operation of the modular multilevel converters," in *Proc. IEEE Energy Convers. Congr. Expo.*, 2015, pp. 4700–4705.
[15] S. Du, B. Wu, K. Tian, N. Zargari, and Z. Cheng, "An active cross-connected modular multilevel converter (AC-MMC) for medium-voltage motor drive," *IEEE Trans. Ind. Electron.*, vol. 63, no. 8, pp. 4707–4717, Aug. 2016.
[16] A. Mertens and J. Kucka, "Quasi two-level PWM operation of an MMC phase leg with reduced module capacitance," *IEEE Trans. Power Electron.*, vol. 31, no. 10, pp. 6765–6769, Oct. 2016.
[17] R. Picas, S. Ceballos, J. Pou, J. Zaragoza, G. Konstantinou, and V. G. Agelidis, "Closed loop discontinuous modulation technique for capacitor voltage ripple and switching losses reduction in modular multilevel converters," *IEEE Trans. Power Electron.*, vol. 30, no. 9, pp. 4714–4725, Sep. 2015.
[18] R. Yang, B. Li, G. Wang, C. Cecati, S. Zhou, and D. Xu, "Asymmetric mode control of MMC to suppress capacitor voltage ripples in low frequency low voltage condition," *IEEE Trans. Power Electron.*, vol. 32, no. 6, pp. 4219–4230, Jun. 2017.
[19] Y. S. Kumar and G. Poddar, "Control of medium-voltage ac motor drive for wide speed range using modular multilevel converter," *IEEE Trans. Ind. Electron.*, vol. 64, no. 4, pp. 2742–2749, Apr. 2017.
[20] Y. S. Kumar and G. Poddar, "Medium-voltage vector control induction motor drive at zero frequency using modular multilevel converter," *IEEE Trans. Ind. Electron.*, vol. 65, no. 1, pp. 125–132, Jan. 2018.
[21] M. S. Diab, B. W. Williams, D. Holliday, A. M. Massoud, and S. Ahmed, "A modular multilevel converter with isolated energy-balancing modules for MV drives incorporating symmetrical six-phase machines," in *Proc. IEEE Energy Convers. Congr. Expo.*, 2017, pp. 2715–2722.
[22] B. Li, S. Zhou, D. Xu, S. J. Finney, and B. W. Williams, "A hybrid modular multilevel converter for medium-voltage variable-speed motor drives," *IEEE Trans. Power Electron.*, vol. 32, no. 6, pp. 4619–4630, Jun. 2017.

Shaoze Zhou (S'17) was born in 1993. He received the B.S. degree in electrical engineering from Hohai University, Nanjing, China, in 2015. He is currently working toward the Ph.D. degree at the Harbin Institute of Technology, Harbin, China.

His research interests include multilevel converters, motor drives, and pulsewidth modulation techniques.

Binbin Li (S'15–M'17) received the B.S., M.S., and Ph.D. degrees in electrical engineering from the Harbin Institute of Technology, Harbin, China, in 2010, 2012, and 2017, respectively.

From 2015 to 2016, he was a Visiting Researcher with the Department of Electronic and Electrical Engineering, University of Strathclyde, Glasgow, U.K. He is currently an Associate Professor with the Department of Electrical Engineering, Harbin Institute of Technology. His research interests include multilevel converters, high-power electronics, control algorithms, and pulsewidth modulation techniques.

Mingxu Guan was born in 1993. He received the B.S. degree in electrical engineering in 2016 from the Harbin Institute of Technology, Harbin, China, where he is currently working toward the M.S. degree.

His research interests include modular multilevel converters, modeling and controls, and motor drives.

Xinyi Zhang was born in 1994. She received the B.S. degree in water conservancy and hydropower engineering in 2015 from Hohai University, Nanjing, China, where she is currently working toward the Ph.D. degree.

Since 2018, she has been a Visiting Researcher with Lund University, Lund, Sweden. Her research interests include hydrology and hydropower station dispatching under climate change.

Zigao Xu (S'17) was born in 1994. He received the B.S. degree in electrical engineering from the Taiyuan University of Technology, Taiyuan, China, in 2016. Since then, he has been working toward the M.S. and Ph.D. degrees at the Harbin Institute of Technology, Harbin, China.

His research interests include multilevel converters, and modeling and control algorithms.

Dianguo Xu (M'97–SM'12–F'17) received the B.S. degree in control engineering from Harbin Engineering University, Harbin, China, in 1982, and the M.S. and Ph.D. degrees in electrical engineering from the Harbin Institute of Technology (HIT), Harbin, in 1984 and 1989, respectively.

In 1984, he became an Assistant Professor with the Department of Electrical Engineering, HIT, where he has been a Professor since 1994. He was the Dean of the School of Electrical Engineering and Automation, HIT, from 2000 to 2010. He is currently the Vice-President of HIT. He has authored or coauthored more than 600 technical papers. His research interests include renewable energy generation technology, multiterminal HVdc system based on voltage source converter (VSC), power quality mitigation, speed sensorless vector controlled motor drives, high-performance PMSM servo system.

Prof. Xu is an Associate Editor for the IEEE TRANSACTIONS ON INDUSTRIAL ELECTRONICS, IEEE TRANSACTIONS ON POWER ELECTRONICS, and the IEEE JOURNAL OF EMERGING AND SELECTED TOPICS IN POWER ELECTRONICS. He also serves as the Chairman of the IEEE Harbin Section.